Diseased Region Detection of Longitudinal Knee MRI Data

Chao Huang[1,3], Liang Shan[2], Cecil Charles[4], Marc Niethammer[2], and Hongtu Zhu[3,⋆]

[1] Department of Mathematics, Southeast University, China
[2] Department of Computer Sciences and Biomedical Research Imaging Center, University of North Carolina at Chapel Hill, USA
[3] Department of Biostatistics and Biomedical Research Imaging Center, University of North Carolina at Chapel Hill, USA
[4] Department of Radiology, Duke University, USA
htzhu@email.unc.edu

Abstract. Statistical analysis of longitudinal cartilage changes in osteoarthritis (OA) is of great importance and still a challenge in knee MRI data analysis. A major challenge is to establish a reliable correspondence across subjects within the same latent subpopulations. We develop a novel Gaussian hidden Markov model (GHMM) to establish spatial correspondence of cartilage thinning across both time and subjects within the same latent subpopulations and make statistical inference on the detection of diseased regions in each OA patient. A hidden Markov random field (HMRF) is proposed to extract such latent subpopulation structure. The EM algorithm and pseudo-likelihood method are both considered in making statistical inference. The proposed model can effectively detect diseased regions and present a localized analysis of longitudinal cartilage thickness within each latent subpopulation. Simulation studies and diseased region detection on 2D thickness maps extracted from full 3D longitudinal knee MRI Data for Pfizer Longitudinal Dataset are performed, which show that our proposed model outperforms standard voxel-based analysis.

Keywords: Diseased regions detection, EM algorithm, Gaussian hidden Markov model, Longitudinal cartilage thickness, Pseudo-likelihood method.

1 Introduction

Osteoarthritis (OA) is the most common form of arthritis and a major cause of longterm disability in the US [18]. It is estimated that more than 16% of all adults 45 years or older suffer from symptomatic OA of the knee [5]. The OA symptoms include swelling, pain, discomfort and problems in mobility and are caused by the progressive loss of joint cartilage [5]. Fig. 1 shows the anatomy of the human knee and illustrates the cartilage loss.

⋆ Corresponding author.

J.C. Gee et al. (Eds.): IPMI 2013, LNCS 7917, pp. 632–643, 2013.
© Springer-Verlag Berlin Heidelberg 2013

Cartilage loss [9] is believed to be the dominating factor in OA. Studying cartilage morphological changes will help understand OA progression and drug development. Magnetic resonance imaging (MRI) is a three-dimensional imaging technique able to directly measure cartilage volume and thickness and is thus sensitive to the detection of cartilage loss. Significant advances in MRI have resulted in the ability to quantify cartilage morphology [8]. Therefore, MRI is increasingly accepted as a primary method to evaluate progression of OA (see [6], [16]). Meanwhile, large image databases have been acquired for OA research. It would be of great value to fully analyze the MR images of the datasets such as the one form the osteoarthritis initiative to help understand the progression of OA.

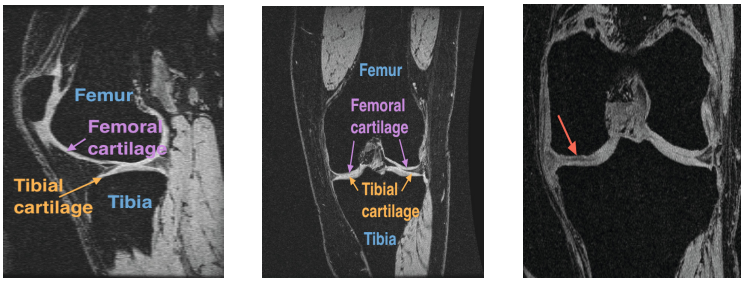

Fig. 1. Anatomy of human knee and illustration of cartilage loss. (*left*) A sagittal slice of a healthy knee. Bones are annotated in blue, femoral cartilage in purple and tibial cartilage in orange. (*middle*) A coronal slice of the same healthy knee. (*right*) A coronal slice of an OA knee with cartilage loss indicated by the red arrow.

Subregion-based analysis is one of the most popular approaches among existing statistical analysis methods (see [4], [17]). However, this approach can be problematic because changes within a specific subregion could happen only to a few subjects within a latent subpopulation whereas other subjects have strong progressions in different subregions and belong to different latent subpopulations. Local changes (that happen to a smaller region than the size of a subregion) are weakened by averaging over a particular subregion and are impossible to recover. So, statistical analysis of cartilage thickness changes is still a challenging problem. To fully understand the spatial pattern of OA progression, the analysis of localized cartilage thickness changes is necessary.

The aim of this paper is to develop a novel Gaussian hidden Markov model (GHMM) to establish spatial correspondence of cartilage thinning across time and subjects within the same subpopulation. A hidden Markov random field (HMRF) is developed to specifically discover the disease regions [2], [14]. The EM algorithm and pseudo-likelihood method are both considered in making statistical inference. The proposed model can can effectively detect diseased regions and presents a localized analysis of longitudinal cartilage thickness. Simulation studies and diseased regions detection of 2D thickness map extracted from full 3D

longitudinal knee MRI Data of the Pfizer Longitudinal Study (PLS-A9001140) are performed, which shows that our proposed model outperforms the classical linear mixed model.

The paper is organized as follows. Section 2 introduces GHMM and then the related EM algorithm for the proposed model is derived. In Section 3, simulation studies are performed to show the advantages of our proposed model in diseased regions detection. Section 4 applies GHMM to the 2D thickness maps derived from the 3D MRI data of the Pfizer Longitudinal Study (PLS-A9001140).

2 Background and Methods

2.1 Gaussian Hidden Markov Model

Suppose that we observe a longitudinal imaging data set with imaging data $\{y_{ij}(s_k) : k = 1, \ldots, m\}$ measured at time t_j for $j = 1, \ldots, T_i$ and $i = 1, \ldots, n$, where $S = \{s_1, \ldots, s_m\}$ is the set of pixels and T_i is the total number of time points for the $i-$th subject. Let x_i represent disease status of osteo-arthritis (OA) for each subject such that $x_i = 0$ and 1, respectively, represent normal control and patient with OA. At each pixel s_k, we introduce an unobserved random effect $b_i(s_k)$ to label normal region R_{i0}, median diseased region R_{i1}, and severely diseased region R_{i2} for each subject. For normal controls, both R_{i1} and R_{i2} should be the empty set. Specifically, $b_i(s_k) \in L = \{0, 1, 2\}$ are label configurations of three nonoverlapping regions $\{R_{i0}, R_{i1}, R_{i2}\}$. Note that these three unknown regions for each subject play a critical role in establishing spatial correspondences across subjects. Moreover, we introduce another unobserved random effect $\boldsymbol{v}_i(s_k)$ to characterize temporal correlations among repeated measures for each subject.

Our Gaussian hidden Markov model consists of a a spatial random effect model (SREM) and a Potts model. We first propose SREM to model the conditional distribution of the observed images given the random effects. Specifically, given $\boldsymbol{b}_i$ and $\boldsymbol{v}_i$, we propose a general spatial random effect model given by

$$y_{ij}(s_k) = \boldsymbol{w}_j^T \boldsymbol{\beta}(s_k) + c(x_i, \boldsymbol{w}_j, b_i(s_k), \bar{\boldsymbol{\beta}}) + \boldsymbol{w}_j^T \boldsymbol{v}_i(s_k) + \epsilon_{ij}(s_k), \tag{1}$$

where $\boldsymbol{w}_j$ is a $q_w \times 1$ vector of covariates (e.g., time) and $\boldsymbol{\beta}(s_k)$ is a q_w dimensional vector of regression coefficients representing the dynamic change of imaging intensities at pixel s_k in normal controls. Moreover, $\bar{\boldsymbol{\beta}} = (\bar{\boldsymbol{\beta}}(1), \bar{\boldsymbol{\beta}}(2))^T$ is a $2q_w$ dimensional vector of coefficients to characterize the dynamic changes of imaging intensities in the diseased region $R_{i1} \cup R_{i2}$. The function $c(x_i, \boldsymbol{w}_j, b_i(s_k), \bar{\boldsymbol{\beta}})$ is defined as

$$c(x_i, \boldsymbol{w}_j, b_i(s_k), \bar{\boldsymbol{\beta}}) = \begin{cases} 0, & x_i = 0, \\ \sum_{l=1}^{2} \boldsymbol{w}_j^T \bar{\boldsymbol{\beta}}(l) \delta(b_i(s_k), l) & , x_i \neq 0. \end{cases} \tag{2}$$

where $\delta(\cdot,\cdot)$ is the Kronecker function. Thus, $c(x_i, \boldsymbol{w}_j, b_i(s_k), \bar{\boldsymbol{\beta}})$ equals zero for all pixels for normal controls and the pixels with $b_i(s_k) = 0$ for OA patients. For OA patients, pixels in different diseased regions may have different dynamic changes of imaging intensities. Throughout the paper, we assume $\boldsymbol{w}_j = (1, t_j, t_j^2)^T$ and set $q_w = 3$. Moreover, $\epsilon_{ij}(s_k)$ are independent measurement errors across subjects, time, and pixels, while they follow $N(0, \sigma^2_{s_k})$.

We model the random effects $\boldsymbol{b}_i$ and $\boldsymbol{v}_i$ as follows. First, it is assumed that $\boldsymbol{b}_i = (b_i(s_1), \ldots, b_i(s_m))^T$ and $\boldsymbol{v}_i = \{\boldsymbol{v}_i(s_k) : k = 1, \ldots, m\}$ are mutually independent. Moreover, $\boldsymbol{v}_i(s_k)$ are mutually independent across pixels and $\boldsymbol{v}_i(s_k)$ follows $N(\boldsymbol{0}, \boldsymbol{\Sigma}_{v_{s_k}})$ at pixel s_k. It is assumed that $\boldsymbol{b}_i$ are independent across subjects and $\boldsymbol{b}_i$ follows a Potts model ([2], [14]), whose Gibbs form is given by

$$p(\boldsymbol{b}_i|\tau) = \exp\{-U(\boldsymbol{b}_i)\tau - \log C(\tau)\}, \tag{3}$$

where $U(b_i) = -\sum_{s_k \sim s_l} \delta(b(s_k), b(s_l))$ and parameter τ, which introduces spatial consistency. $C(\tau)$ is the partition function such that $p(\boldsymbol{b}_i|\tau)$ is a probability function. The notation "$\sum_{s_i \sim s_j}$" means that s_i is a neighbor of s_j and each neighboring pair enters the summation only once. Throughout the paper, we only consider the closest neighbors for each pixel.

2.2 Estimation Procedure

Our primary problem of interest is to make inference on all unknown parameters, denoted as $\boldsymbol{\theta}$, and random effects. We decompose the parameter $\boldsymbol{\theta}$ into two parts: τ, introduced in (3), and all others, denoted as $\overline{\boldsymbol{\theta}}$. This is a standard incomplete-data problem. Since the Maximum likelihood estimation (MLE) of τ is generally difficult to compute due to the normalizing part of the probability function in (3), the MLE of $\overline{\boldsymbol{\theta}}$ can be calculated by using the EM algorithm [7], whereas τ can be estimated by using a pseudo-likelihood method [1], which is easy to compute.

Let $\boldsymbol{W}_i = (\boldsymbol{w}_1, \ldots, \boldsymbol{w}_{T_i})$, $\bar{\boldsymbol{c}}(x_i, \boldsymbol{W}_i, b_i(s_k), \bar{\boldsymbol{\beta}}) = (c(x_i, \boldsymbol{w}_1, b_i(s_k), \bar{\boldsymbol{\beta}}), \ldots, c(x_i, \boldsymbol{w}_{T_i}, b_i(s_k), \bar{\boldsymbol{\beta}}))^T$, and $\boldsymbol{\Sigma}_{s_k,i} = \{\kappa_{p,q}\}_{1 \le p,q \le T_i}$, where $\kappa_{p,q} = \sigma^2_{s_k} \mathbf{1}(p = q)$, in which $\mathbf{1}(\cdot)$ is an indicator function. Thus, the distribution of $\boldsymbol{y}_i(s_k)$ conditional on random effects is given by $N(\boldsymbol{z}_i(s_k), \boldsymbol{\Sigma}_{s_k,i})$, where

$$\boldsymbol{z}_i(s_k) = \boldsymbol{y}_i(s_k) - \boldsymbol{W}_i^T \boldsymbol{\beta}(s_k) - \bar{\boldsymbol{c}}(x_i, \boldsymbol{W}_i, b_i(s_k), \bar{\boldsymbol{\beta}}) - \boldsymbol{W}_i^T \boldsymbol{v}_i(s_k),$$

Thus, the complete-data log-likelihood function is given by

$$\begin{aligned} \log \tilde{L}(\boldsymbol{\theta}) \propto & -\frac{1}{2}\sum_{i=1}^{n}\sum_{k=1}^{m} \log|\boldsymbol{\Sigma}_{s_k,i}| - \frac{1}{2}\sum_{i=1}^{n}\sum_{k=1}^{m} \boldsymbol{z}_i(s_k)^T \boldsymbol{\Sigma}^{-1}_{s_k,i} \boldsymbol{z}_i(s_k) - \sum_{i=1}^{n_0} U(\boldsymbol{b}_i)\tau \\ & -n_0 \log C(\tau) - \frac{n}{2}\sum_{k=1}^{m} \log|\boldsymbol{\Sigma}_{v_{s_k}}| - \frac{1}{2}\sum_{i=1}^{n}\sum_{k=1}^{m} \boldsymbol{v}_i^T(s_k) \boldsymbol{\Sigma}^{-1}_{v_{s_k}} \boldsymbol{v}_i(s_k), \end{aligned} \tag{4}$$

where $n_0 = \#\{x_i : x_i \neq 0\}$ denotes the number of OA patients. Given the current estimate $\widetilde{\boldsymbol{\theta}}^{(r)}$ at iteration r, the value $\widetilde{\overline{\boldsymbol{\theta}}}^{(r+1)}$ is obtained via maximizing the Q-function $E_{\widetilde{\theta}^{(r)}}(\log \tilde{L}(\boldsymbol{\theta})|\boldsymbol{y}, \boldsymbol{x})$ with respect to $\overline{\boldsymbol{\theta}}$.

We consider the E-step and M-step of EM algorithm as follows.

E-step: In E-step, we need to calculate four conditional expectations

$$E\big[\boldsymbol{v}_i(s_k)\delta(b_i(s_k),l)\big|\boldsymbol{y}_i(s_k),\boldsymbol{x},\widetilde{\boldsymbol{\theta}}^{(r)}\big], E\big[\boldsymbol{v}_i(s_k)\boldsymbol{v}_i^T(s_k)\big|\boldsymbol{y}_i(s_k),\boldsymbol{x},\widetilde{\boldsymbol{\theta}}^{(r)}\big],$$

$$E\big[\boldsymbol{v}_i(s_k)\big|\boldsymbol{y}_i(s_k),\boldsymbol{x},\widetilde{\boldsymbol{\theta}}^{(r)}\big], E\big[\delta(b_i(s_k),l)\big|\boldsymbol{y}_i(s_k),\boldsymbol{x},\widetilde{\boldsymbol{\theta}}^{(r)}\big].$$

In order to calculate these conditional probability, the class labels $\boldsymbol{b}$ should be estimated first. The MRF-MAP estimation is adopted here. First, the conditional probability density function of $\boldsymbol{y}_i(s_k)$ given x_i and $\boldsymbol{b}_i(s_k)$ is derived as

$$f(\boldsymbol{y}_i(s_k)|x_i,b_i(s_k),\widetilde{\boldsymbol{\theta}}^{(r)}) \sim \mathcal{N}(\boldsymbol{\varpi}_i(s_k),\boldsymbol{W}_i^T\widetilde{\boldsymbol{\Sigma}}_{v_{s_k}}^{(r)}\boldsymbol{W}_i+\widetilde{\boldsymbol{\Sigma}}_{s_k,i}^{(r)}). \tag{5}$$

where $\boldsymbol{\varpi}_i(s_k)=\boldsymbol{W}_i^T\widetilde{\boldsymbol{\beta}}^{(r)}(s_k)+\bar{\boldsymbol{c}}(x_i,\boldsymbol{W}_i,b_i(s_k),\widetilde{\bar{\boldsymbol{\beta}}}^{(r)})$.

According to the MAP criterion, the estimate $\widetilde{\boldsymbol{b}}_i^{(r)}$ is defined as

$$\widetilde{\boldsymbol{b}}_i^{(r)}=\arg\max_{\boldsymbol{b}_i}\left\{\prod_{k=1}^{m}f(\boldsymbol{y}_i(s_k)|x_i,b_i(s_k),\widetilde{\boldsymbol{\theta}}^{(r)})p(\boldsymbol{b}_i|\widetilde{\tau}^{(r)})\right\}. \tag{6}$$

To obtain the optimal solution to (6), in this paper, we adopt the iterated conditional modes (ICM) algorithm proposed by [2]. As a result, the conditional expectation $E\Big[\delta(b_i(s_k),l)\Big|\boldsymbol{y}_i(s_k),\boldsymbol{x},\widetilde{\boldsymbol{\theta}}^{(r)}\Big]$ can be calculated. Then, the desired expectations can be estimated respectively.

M-step: We find the updates of $\overline{\boldsymbol{\theta}}$ as follows. For $\boldsymbol{\beta}(s_k)$ and $\overline{\boldsymbol{\beta}}(l)$, we have

$$\begin{aligned}\widetilde{\boldsymbol{\beta}}^{(r+1)}(s_k)=[\sum_{i=1}^{n}\boldsymbol{W}_i\widetilde{\boldsymbol{\Sigma}}_{s_k,i}^{(r)^{-1}}\boldsymbol{W}_i^T]^{-1}\sum_{i=1}^{n}\boldsymbol{W}_i\widetilde{\boldsymbol{\Sigma}}_{s_k,i}^{(r)^{-1}}\Big(\boldsymbol{y}_i(s_k)-\boldsymbol{W}_i^TE\Big[\boldsymbol{v}_i(s_k)\Big|\boldsymbol{y}_i(s_k),\\ \boldsymbol{x},\widetilde{\boldsymbol{\theta}}^{(r)}\Big]-\delta(x_i,0)\boldsymbol{W}_i^T\sum_{l=1}^{M}\bar{\boldsymbol{\beta}}(l)E\Big[\delta(b_i(s_k),l)\Big|\boldsymbol{y}_i(s_k),\boldsymbol{x},\widetilde{\boldsymbol{\theta}}^{(r)}\Big]\Big),\end{aligned} \tag{7}$$

$$\begin{aligned}\widetilde{\bar{\boldsymbol{\beta}}}^{(r+1)}(l)=\Big[\sum_{i=1}^{n_0}\sum_{k=1}^{m}\boldsymbol{W}_i\widetilde{\boldsymbol{\Sigma}}_{s_k,i}^{(r)^{-1}}\boldsymbol{W}_i^TE\big[\delta(b_i(s_k),l)\big|\boldsymbol{y}_i(s_k),\boldsymbol{x},\widetilde{\boldsymbol{\theta}}^{(r)}\big]\Big]^{-1}\sum_{i=1}^{n_0}\sum_{k=1}^{m}\boldsymbol{W}_i\widetilde{\boldsymbol{\Sigma}}_{s_k,i}^{(r)^{-1}}\\ \Big\{\boldsymbol{y}_i(s_k)-\boldsymbol{W}_i^T\widetilde{\boldsymbol{\beta}}^{(r)}(s_k)-\boldsymbol{W}_i^TE\Big[\boldsymbol{v}_i(s_k)\delta(b_i(s_k),l)\Big|\boldsymbol{y}_i(s_k),\boldsymbol{x},\widetilde{\boldsymbol{\theta}}^{(r)}\Big]\Big\}.\end{aligned} \tag{8}$$

For the covariance matrix $\boldsymbol{\Sigma}_{v_{s_k}}$, we have

$$\widetilde{\boldsymbol{\Sigma}}_{v_{s_k}}^{(r+1)}=\frac{1}{n}\sum_{i=1}^{n}E\Big[\boldsymbol{v}_i(s_k)\boldsymbol{v}_i^T(s_k)\Big|\boldsymbol{y}_i(s_k),\boldsymbol{x},\widetilde{\boldsymbol{\theta}}^{(r)}\Big], \tag{9}$$

For $\sigma_{s_k}^2$ and ρ_{s_k}, we have

$$\widetilde{\sigma}_{s_k}^{2(r+1)} = \frac{1}{\sum_{i=1}^{n} T_i} \sum_{i=1}^{n} E\Big[[\widetilde{\boldsymbol{L}}_i^{(r)} \boldsymbol{z}_i^{(r)}(s_k)]^T \widetilde{\boldsymbol{L}}_i^{(r)} \boldsymbol{z}_i^{(r)}(s_k) \Big| \boldsymbol{y}_i(s_k), \boldsymbol{x}, \widetilde{\boldsymbol{\theta}}^{(r)}\Big], \quad (10)$$

$$\widetilde{\rho}_{s_k}^{(r+1)} = \Big[\sum_{i=1}^{n} E\Big[[\boldsymbol{z}_i^{(r)}(s_k)]^T \boldsymbol{K}_i \boldsymbol{z}_i^{(r)}(s_k) \Big| \boldsymbol{y}_i(s_k), \boldsymbol{x}, \widetilde{\boldsymbol{\theta}}^{(r)}\Big]\Big]^{-1} \sum_{i=1}^{n} E\Big[[\boldsymbol{z}_i^{(r)}(s_k)]^T \boldsymbol{R}_i \boldsymbol{z}_i^{(r)}(s_k) \Big| \boldsymbol{y}_i(s_k), \boldsymbol{x}, \widetilde{\boldsymbol{\theta}}^{(r)}\Big], \quad (11)$$

where $\boldsymbol{z}_i^{(r)}(s_k) = \boldsymbol{y}_i(s_k) - \boldsymbol{W}_i^T \widetilde{\boldsymbol{\beta}}^{(r)}(s_k) - \bar{\boldsymbol{c}}(x_i, \boldsymbol{W}_i, b_i(s_k), \widetilde{\bar{\boldsymbol{\beta}}}^{(r)}) - \boldsymbol{W}_i^T \boldsymbol{v}_i(s_k)$, and $\widetilde{\boldsymbol{L}}_i^{(r)}$, $\boldsymbol{K}_i$ and $\boldsymbol{R}_i$ are given by

$$\widetilde{\boldsymbol{L}}_i^{(r)} = \begin{bmatrix} 1 & 0 & \cdots & 0 \\ -\widetilde{\rho}_{s_k}^{(r)} & 1 & \cdots & 0 \\ \vdots & \ddots & \ddots & \vdots \\ 0 & \cdots & -\widetilde{\rho}_{s_k}^{(r)} & 1 \end{bmatrix}_{T_i}, \boldsymbol{K}_i = \begin{bmatrix} 1 & 0 & \cdots & 0 \\ 0 & \ddots & \cdots & 0 \\ \vdots & \ddots & 1 & \vdots \\ 0 \cdots & & 0 & 0 \end{bmatrix}_{T_i}, \boldsymbol{R}_i = \begin{bmatrix} 0 & 0 & \cdots & 0 \\ 1 & \ddots & \cdots & 0 \\ \vdots & \ddots & \cdots & \vdots \\ 0 \cdots & & 1 & 0 \end{bmatrix}_{T_i}.$$

The parameter τ in MRF model (3) is estimated based on a pseudo-likelihood method. The pseudo-likelihood at the rth step is a simple product of the conditional likelihood

$$PL(\widetilde{\boldsymbol{b}}^{(r)}) = \prod_{i=1}^{n_0} \prod_{s_k \in \mathcal{S} - \partial\mathcal{S}} PL(\widetilde{b}_i^{(r)}(s_k) | \widetilde{\boldsymbol{b}}_i^{(r)}), \quad (12)$$

where $\partial\mathcal{S}$ denotes the set of points at the boundaries of $\mathcal{S}$. The pseudo-likelihood does not involve the partition function. Although the pseudo-likelihood is not the true likelihood function, the maximum pseudo-likelihood (MPL) estimate converges to the truth with probability one [10]. The logarithm pseudo-likelihood is given by

$$\ln PL(\widetilde{\boldsymbol{b}}^{(r)}, \tau) = \sum_{i=1}^{n_0} \sum_{s_k \in \mathcal{S} - \partial\mathcal{S}} \ln \Big[PL(\widetilde{b}_i^{(r)}(s_k) | \widetilde{\boldsymbol{b}}_i^{(r)})\Big], \quad (13)$$

Thus, the MPL estimate $\widetilde{\tau}^{(r+1)}$ can be obtained by solving

$$\frac{\partial \ln PL(\widetilde{\boldsymbol{b}}^{(r)}, \tau)}{\partial \tau} = 0. \quad (14)$$

The E-step and M-step are alternately repeated until the difference between $\log L(\widetilde{\boldsymbol{\theta}}^{(r+1)})$ and $\log L(\widetilde{\boldsymbol{\theta}}^{(r)})$ is smaller than a desired small value (e.g., 0.0001).

3 Simulation Studies

We examine the finite sample performance of GHMM for diseased region detection. We chose the femoral cartilage thickness data of all the normal controls derived from the 3D MRI data of the Pfizer Longitudinal Study (PLS-A9001140) and fitted the model (1) to all MRI data obtained from normal controls. We set the obtained parameter estimators as the true values of parameters $\boldsymbol{\beta}(s_k), \boldsymbol{\Sigma}_{v_{s_k}}, \sigma^2_{s_k}$ and ρ_{s_k}. The related parameter $\overline{\boldsymbol{\beta}}(l)$ are generated from $U(-0.1, 0.1)$ and $U(-0.5, 0.5)$ for $l = 1, 2$, respectively. The parameter τ was set as 0.5. The covariate $\boldsymbol{W}_i$ for each subject was generated according to the real dataset in Section 4. We generated 20 subjects from 3 groups with 7 subjects in group 1, 7 subjects in group 2, and 6 subjects in group 3. The location of the diseased region is predetermined and does not vary for subjects in the same group, whereas it varies across groups. These three kinds of the diseased regions are shown in Fig. 2.

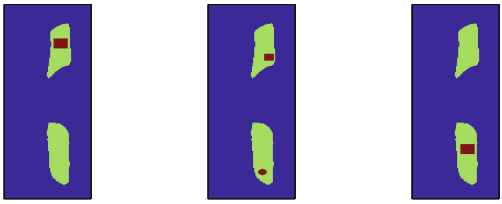

Fig. 2. Three kinds of the diseased regions: diseased region (*red*); normal region (*green*)

We applied GHMM to detect the diseased region in each subject. We randomly selected one subject from each group and presented its detection results in Fig. 3. For all selected subjects, the diseased regions can be successfully detected with few misclassifications in the results. To show the average detection performance among subjects in each group, the Dice metric [13], Rand index [15], adjusted Rand index, and Mirkin metric [11] were calculated to compare the detection results with the truth and the average of each index values were also calculated. For the first three indexes, a higher index value indicates a more accurate detection result, while it is the opposite case for the last index. Simulation results based on all the three groups are presented in Table 1. For all these groups, the average of the first three index values are larger than 88 percent, and the last index values are all less than 0.1. Fig. 3 and Table 1 indicate that GHMM performs very well in diseased region detection of cartilage MRI data.

4 Real Data Analysis

We consider the dataset of the Pfizer longitudinal study on osteoarthritis (PLS-A9001140). This dataset contains T1-weighted (3D SPGR) images for

Table 1. Average detection performance among subjects in different groups

	Dice metric	Rand index	Adjusted Rand index	Mirkin metric
Group 1	0.9818	0.9643	0.9008	0.0357
Group 2	0.9797	0.9602	0.8874	0.0398
Group 3	0.9688	0.9395	0.8802	0.0605

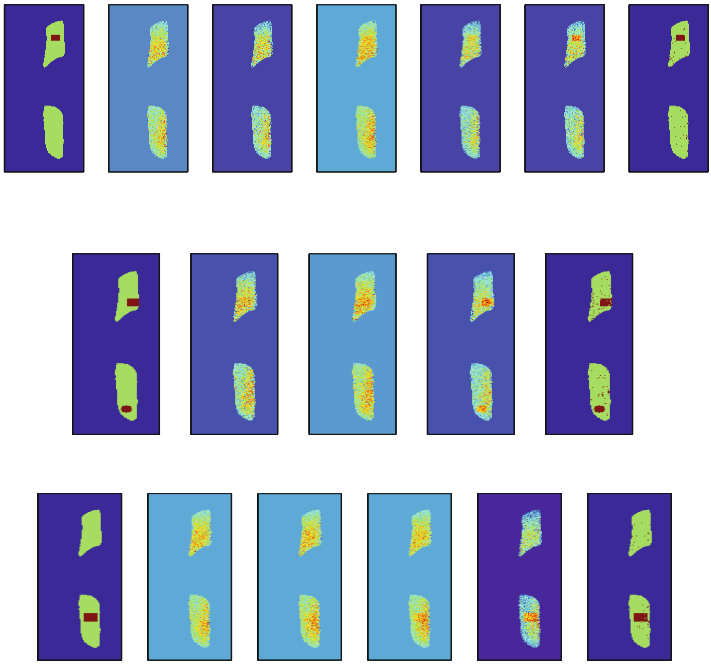

Fig. 3. Diseased region detection for subjects from three groups: subject with 5 time points in group 1 (*top*); subject with 3 time points in group 2 (*middle*); subject with 4 time point in group 3 (*bottom*). This is the simulated result and hence we have an imposed ground truth. In each group, the first image presents the true diseased region while the last image indicate the detection result, the remaining ones are the observations for the time points.

155 subjects, imaged at baseline, 3, 6, 12, and 24 months at a resolution of $1.00 \times 0.31 \times 0.31mm^3$. Some subjects have missing scans and thus we have 706 MRIs in total. The Kellgren-Lawrence grades (KLG) [12] were determined for all subjects from the baseline scan, classifying 81 as normal control subjects (KLG0), 1 as KLG1 (mild OA), 40 as KLG2 (severe OA) and 33 as KLG3 (severe OA).

We applied a voxel-based analysis based on linear mixed models and GHMM to the OA data set. Moreover, the expert cartilage segmentations are available for all images in the native image space. The femoral cartilage segmentation was

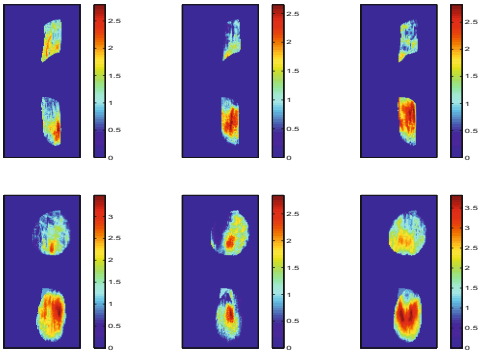

Fig. 4. Local cartilage thickness (mm) for subjects with expert segmentations at baseline with different KLG: (*left*) femoral cartilage thickness map(*top*) and tibial cartilage thickness map(*bottom*) for subject with KLG0; (*middle*) femoral cartilage thickness map(*top*) and tibial cartilage thickness map(*bottom*) for subject with KLG1; (*left*) femoral cartilage thickness map(*top*) and tibial cartilage thickness map(*bottom*) for subject with KLG3.

drawn only on the weight-bearing part, whereas the tibial cartilage segmentation covers the entire region. We randomly chose several subjects with different KLG from the dataset, and present the related cartilage segmentations for the chosen subjects at baseline in Fig. 4.

Firstly, we applied the voxel-based analysis to the MRI data from normal controls and calculated the estimated average thickness at each pixel site. Secondly, we applied the voxel-based analysis to the whole dataset and then calculated the estimated average thickness at each pixel site. We carried out a t test across pixels to identify whether the estimated thickness of each diseased patient is significantly different from the estimated average thickness obtained from normal controls. If the hypothesis is rejected at a given pixel at a significance level 1%, then this pixel site is treated as the one from the disease region. Otherwise, it belongs to the normal region. Fig. 4 presents several randomly chosen subjects with KLG1 and KLG3, whereas Fig. 5 presents the related p-value at each pixel site. As a comparison, we applied GHMM to the whole dataset. The detection results of the two selected subjects are also plotted in Fig. 6, where the red area indicates the diseased region while the green one indicates the normal region. The probability that a pixel site comes from the diseased region can also be estimated. The empirical probability distribution of the diseased region based on GHMM and the voxel-based analysis are both presented in Fig. 7. From Fig. 5-Fig. 7, it follows that the p-value at most pixel sites is not significant and thus the voxel-based analysis fails to realize the diseased region detection. In contrast, for GHMM, the detected diseased regions probably locate in the center of the cartilage, which means that the cartilage loss in OA may not be uniform throughout the cartilage, but OA may affect certain regions (e.g. the center) more frequently than other regions [3]. Therefore, GHMM outperforms

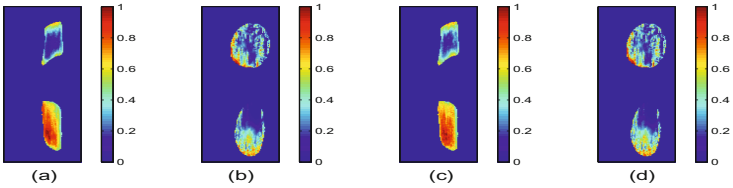

Fig. 5. P-value at each pixel site for subjects randomly chosen with different KLG: (a) p-value in femoral cartilage of subject with KLG1; (b) p-value in tibial cartilage of subject with KLG1; (c) p-value in femoral cartilage of subject with KLG3; (d) p-value in tibial cartilage of subject with KLG3.

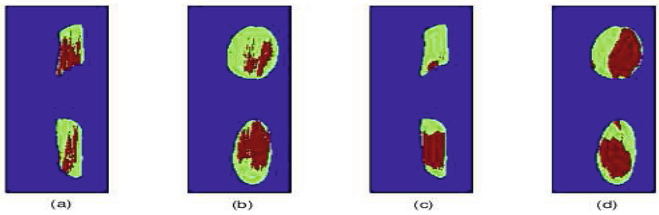

Fig. 6. Diseased region detection for subjects randomly chosen with different KLG: (a) diseased region (red) in femoral cartilage of subject with KLG1; (b) diseased region (red) in tibial cartilage of subject with KLG1; (c) diseased region (red) in femoral cartilage of subject with KLG3; (d) diseased region (red) in tibial cartilage of subject with KLG3.

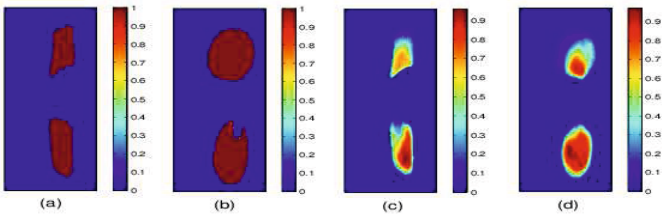

Fig. 7. Empirical probability distribution of the diseased region: (a) empirical probability distribution of the diseased region in femoral cartilage based on the voxel-based analysis; (b) empirical probability distribution of the diseased region in tibial cartilage based on the voxel-based analysis; (c) empirical probability distribution of the diseased region in femoral cartilage based on GHMM; (d) empirical probability distribution of the diseased region in tibial cartilage based on GHMM.

the voxel-based analysis in localized analysis of longitudinal cartilage thickness and diseased region detection.

5 Concluding Remarks

We have developed a novel GHMM to establish spatial correspondence of cartilage thinning across time and subjects within the same latent subpopulation. A hidden Markov random field (HMRF) has been proposed to extract such latent subpopulation structure. Simulation studies and real data analysis demonstrate that GHMM can effectively realize diseased regions detection in localizing longitudinal cartilage thickness. However, one would like to estimate the continuous level of disease, i.e., from completely healthy to fully diseased. Thus, more research on this issue will be valuable and we believe this is an interesting direction for further exploration.

Acknowledgments. This work was supported in part by NIH grants R025747-01, CA142538-01, MH086633, B005149-01, R01 MH091645-01A1, R21 AR059890, and the Pfizer longitudinal study on osteoarthritis (PLS-A9001140).

References

1. Besag, J.E.: Statistical Analysis of Non-Lattice Data. Journal of Royal Statistical Society, Series D 24, 179–195 (1975)
2. Besag, J.E.: On the statistical analysis of dirty pictures (with discussion). Journal of Royal Statistical Society, Series B 48, 259–302 (1986)
3. Biswal, S., Hastie, T., Andriacchi, T.P., Bergman, G.A., Dillingham, M.F., Lang, P.: Risk factors and progressive cartilage loss in the knee: A longitudinal magnetic resonance imaging study in forty-three patients. Arthritis & Rheumatism 46, 2884–2892 (2002)
4. Buck, R.J., Wyman, B.T., Graverrand, M.P.L., Hudelmaier, M., Wirth, W., Ecksten, F.: Does the use of ordered values of subregional change in cartilage thickness improve the detection of disease progression in longitudinal studies of osteoarthritis? Arthritis and Rheumatism 61(7), 917–924 (2009)
5. Arthritis related statistics, Center of Disease Control, CDC (2008), `http://www.cdc.gov/arthritis/data_statistics/arthritis_related_statistics.htm`
6. Cicuttini, F., Hankin, J., Jones, G., Wluka, A.: Comparison of conventional standing knee radiographs and magnetic resonance imaging in assessing progression of tibiofemoral joint osteoarthritis. Oesteoarthritis Cartilage 13, 722–727 (2005)
7. Dempster, A.P., Laird, N.M., Rubin, D.B.: Maximum likelihood from incomplete data via the EM algorithm (with discussion). J. R. Stat. Soc. Series B 39(1), 1–38 (1977)
8. Eckstein, F., Cicuttini, F., Raynauld, J.P., Waterton, J.C., Peterfy, C.: Magnetic resonance imaging (MRI) of articular cartilage in knee osteoarthritis (OA): morphological assessment. Osteoarthritis and Cartilage 14, A46–A75 (2006)
9. Felson, D.T., Lawrence, R.C., Dieppe, P.A., Hirsch, R., Helmick, C.G., Jordan, J.M., Kington, R.S., Lane, N.E., Nevitt, M.C., Zhang, Y., Sowers, M., McAlindon, T., Spector, T.D., Poole, A.R., Yanovski, S.Z., Ateshian, G., Sharma, L., Buckwalter, J.A., Brandt, K.D., Fries, J.F.: Osteoarthritis: new insights, part 1: the disease and risk factors. Annals of Internal Medicine 133(8), 635–646 (2000)

10. Geman, S., Graffigne, C.: Markov random field image models and their applications to computer vision. In: Proceedings of the International Congress of Mathematicians: Berkeley, pp. 1496–1517 (1987)
11. Hubert, L., Arabie, P.: Comparing partitions. J. Classif. 2, 193–218 (1985)
12. Kellgren, J., Lawrence, J.: Radiological assessment of osteoarthritis. Annals of Rheumatic Diseases 16(4), 494–502 (1957)
13. Lynch, M., Ghita, O., Whelan, P.F.: Segmentation of the left ventricle of the heart in 3-D+t MRI data using an optimized nonrigid temporal model. IEEE Trans. Med. Imaging 27(2), 195–203 (2008)
14. Qian, W., Titterington, D.M.: Estimation of parameters in hidden Markov models. Philosophical Transactions of the Royal Society of London, Series A 337, 407–428 (1991)
15. Rand, W.M.: Objective criteria for the evaluation of clustering methods. J. Am. Stat. Assoc. 66, 846–850 (1971)
16. Raynauld, J.P.: Quantitative magnetic resonance imaging of articular cartilage in knee osteoarthritis. Current Opinions in Rheumatology 15(5), 647–650 (2003)
17. Wirth, W., Eckstein, F.: A technique for regional analysis of femorotibial cartilage thickness based on quantitative magenetic resonance imaging. IEEE Transactions on Medical Imaging 27(6), 737–744 (2008)
18. Woolf, A.D., Pfleger, B.: Burden of major musculoskeletal conditions. Bulletin of the World Health Organization 81, 646–656 (2003)
19. Zhang, Y., Brady, M., Smith, S.: Segmentation of brain MR images through a hidden Markov random field model and the expectation-maximization algorithm. IEEE Transactions on Medical Imaging 15, 45–57 (2001)